^{139}La NMR investigation of spin ordering in $La_{0.5}Ca_{0.5}MnO_3$

G. Papavassiliou, M. Fardis, F. Milia, A. Simopoulos, G. Kallias, M. Pissas, D. Niarchos, and N. Ioannidis
NCSR ''Demokritos'' Institute of Materials Science, 153 10 Ag. Paraskevi Attiki, Athens, Greece

C. Dimitropoulos
Institut de Physique Experimentale, EPFL-PH-Ecublens, 1015-Lausanne, Switzerland

J. Dolinsek
''Josef Stefan'' Institute, Jamova 39, 61111 Ljubljana, Slovenia
(Received 30 January 1997)

^{139}La NMR in a zero external magnetic field has been used as a probe in order to study the Mn spin ordering of $La_{0.5}Ca_{0.5}MnO_3$. For $T<T_c$ two different spin configurations are detected, assigned to a ferromagnetic and an antiferromagnetic one, which persist down to the lowest measured temperature $T=90$ K. Close to T_c strong coherent spin fluctuations are detected that presumably drive the paramagnetic-to-ferromagnetic phase transition. Complementary magnetic and Mn^{4+} electron paramagnetic resonance measurements are in agreement with the NMR results. [S0163-1829(97)04221-5]

I. INTRODUCTION

Doped members of the $LaMnO_3$ family with the general formula $A_{1-x}B_xMnO_3$ ($A=La^{3+},Pr^{3+}$, $B=Ca^{2+}$, Sr^{2+},Ba^{2+}) attain currently a lot of theoretical and experimental interest, due to the close relation between magnetic and transport properties. For doping concentration $0.2\leqslant x \leqslant 0.5$ these materials exhibit a paramagnetic (PM) to ferromagnetic (FM) phase transition associated with a sharp drop of resistivity. The transport properties can be controlled by an external magnetic field, thus resulting in the appearance of a large negative magnetoresistance with a maximum at temperatures close to the transition temperature T_c. For $x>0.5$ the low-temperature phase is insulating and antiferromagnetic (AFM), whereas in a narrow range around $x=0.5$, by decreasing temperature, the phase transition route is PM→FM→AFM.[1] Investigations on $Pr_{0.5}Sr_{0.5}MnO_3$ (Ref. 2) and $La_{0.5}Ca_{0.5}MnO_3$ (Refs. 3 and 4) have shown that in this concentration range, charge ordering (CO) effects, i.e., the regular arrangement of Mn^{3+}:Mn^{4+} in 1:1 ratio, plays an important role in the electronic and magnetic properties.

Conventionally, such a PM-FM phase transition is explained by the double exchange (DE) interaction model,[5] according to which the motion of e_g electrons mediates a FM interaction among localized t_{2g} spins, due to Hunds's rule coupling. However, as Millis, Littlewood, and Shraiman pointed out[6] the predictions of the DE model do not fit properly with many aspects of the experimental data, especially with the temperature dependence of the resistivity. Instead of this, they proposed a generalized model which includes electron-lattice coupling in order to explain the appearance of the colossal magnetoresistance. Besides, the relation between the DE interaction and the incommensurate CO superstructure, observed in the FM phase of $La_{0.5}Ca_{0.5}MnO_3$,[4] is at present unclear. According to electron-diffraction experiments[4] for $T_N<T<T_c$ the wave vector of the charge modulation can be written as $q=(2\pi/a)(\frac{1}{2}-\delta,0,0)$, whereas $\delta\rightarrow 0$ for $T\rightarrow T_N$. These results are well correlated with synchroton x-ray experiments,[7] which show an unusual peak broadening starting at T_c and terminating at T_N.

CO is widely accepted to be connected with the complicated spin lattice. Neutron diffraction experiments[8] and theoretical predictions[9] performed on the $x=0.5$ system show that the low-temperature AFM spin structure, known as CE structure, consists of stacked Mn spin cells of the *C* and *E* type, with alternatively parallel and antiparallel spins on successive (100) planes. However, the neutron diffraction data are not uniquely verified by this complex configuration, and perhaps more detailed experiments are necessary in order to predict precisely the spin structure.

In order to gain more understanding on the relevance between charge and magnetic ordering, we performed ^{139}La NMR measurements in a zero external magnetic field complemented by electron paramagnetic resonance (EPR) and magnetic measurements on polycrystalline $La_{0.5}Ca_{0.5}MnO_3$.

II. EXPERIMENTAL AND SAMPLE CHARACTERIZATION

A sample with nominal composition $La_{0.5}Ca_{0.5}MnO_3$ was prepared by thoroughly mixing high-purity stoichiometric amounts of La_2O_3, $CaCO_3$, and MnO_2. The mixed powder was pelletized and annealed in air at 1300 °C for 4 days with intermediate grinding and reformation into pellets each time. Finally the sample was slowly cooled to room temperature by turning off the furnace.

X-ray powder diffraction (XRD) data were collected with D500 SIEMENS diffractometer, using Cu $K\alpha$ radiation and a graphite crystal monochromator, from 4° to 120° in steps of 0.03° in 2θ. The power conditions were set at 40 kV/35 mA. The aperture slit as well as the soller slit were set at 1°. Rietveld lattice parameters were determined to be $a=5.410$ Å, $b=7.621$ Å, and $c=5.417$ Å, in closed agreement with published data. Magnetization (M) data were recorded using a commercial superconducting quantum inter-

 © 1997 The American Physical Society

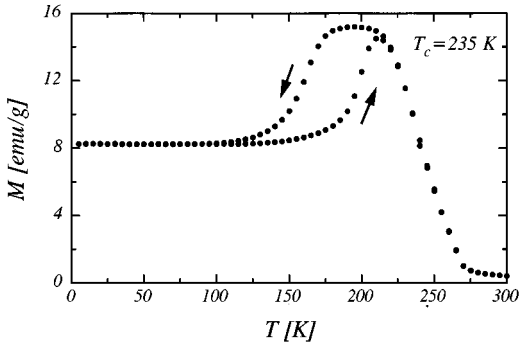

FIG. 1. Magnetization vs temperature for $La_{0.5}Ca_{0.5}MnO_3$. Arrows indicate cooling and heating of the sample.

ference device magnetometer at $B=1000$ G.

The NMR spectra were obtained on a Bruker 200 MSL spectrometer equipped with an Oxford cryostat, by using a spin-echo technique with pulse widths $t_{p1}=t_{p2}=0.6$ μsec and at very-low rf power levels ($B_1<8$ G), due to the very strong rf enhancement factor which is characteristic for magnetic materials.[10,11] The EPR measurements were performed on a Bruker ER 200D-SRC spectrometer with an Oxford ESR 9 cryostat, at modulation amplitude 25 G, microwave power 33 mW, and microwave frequency 9.4 GHz.

III. EXPERIMENTAL RESULTS

Figure 1 shows M versus T curves both upon cooling and warming. By decreasing temperature the system undergoes a PM-FM transition at $T_c=235$ K defined as the inflection point of the magnetization curve. M is observed to saturate at $T\approx 210$ K, while it starts dropping at $T_N\approx 175$ K to a non-fully-AFM state falling finally to the 60% of the saturation value. This second transition temperature varies $\sim$30 K between cooling and warming, exhibiting a large hysteresis loop. Similar results have been previously obtained by other workers.[1,7] A careful comparison of Fig. 1 with their results indicates that most probably the dopant concentration in the examined samples lies between $0.48\leqslant x\leqslant 0.50$.

Figure 2 demonstrates ^{139}La NMR spectra at characteristic temperatures in both the FM and AFM phases. Due to the strong hysteresis effects, all measurements were performed upon cooling. In most temperatures, the signals are double peaked, and more than 5 MHz broad, so that only the central $-\frac{1}{2}\rightarrow\frac{1}{2}$ transition is observed (^{139}La has a nuclear spin $I=\frac{7}{2}$).

The origin of the ^{139}La NMR signal is not quite clear. In a recent work on other $LaMnO_3$ based materials,[12] it has been attributed to a transferred hyperfine interaction via the conducting e_g electrons. In our opinion, this is not possible, as the corresponding molecular orbitals which are σ-bonded with O are not directed to the La sites. Furthermore, it has been considered[12] that the hyperfine field is zero in the AFM phase. This consideration is also not valid as indicated by our experiments.

The appearance of a relatively strong local magnetic field at the position of the non magnetic La ion can be described by the nuclear Hamiltonian,

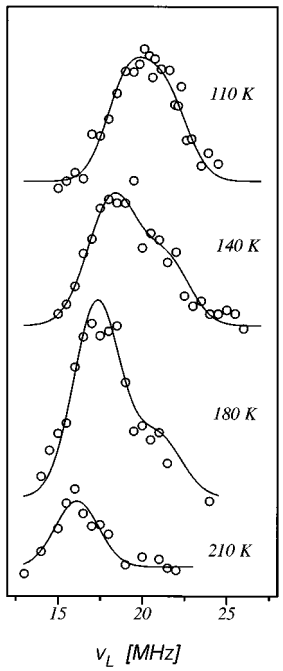

FIG. 2. ^{139}La NMR spectra in a zero external magnetic field at characteristic temperatures.

$$H=\mathbf{I}\sum \hat{A}\mathbf{S}+c\sum_i \mathbf{I}\hat{g}\mathbf{S}\frac{(3\cos^2\theta_i-1)}{r_i^3}, \qquad (1)$$

where the first term concerns the hyperfine interaction between the ^{139}La nuclear spin I and the Mn t_{2g} electron spin S, and the second term the dipolar interaction of I with all the Mn neighbors. The hyperfine interaction probably arises indirectly from π type overlapping between the Mn t_{2g} $|3d_{xy}\rangle$, $|3d_{yz}\rangle$, $|3d_{zx}\rangle$ and the ligand $|2p_\pi\rangle$ wave functions. Similar overlaps of Hartree-Fock Mn^{2+} $|3d_{zx}\rangle$ orbitals with the $|2p_x\rangle$ Slater function of the F^- ions in $KMnF_3$ with almost the same lattice spacing have been calculated in Ref. 13. Since spin-up and spin-down ligand states have different overlapping integrals with the Mn $3d$ states, i.e., $\langle 2p_\pi\uparrow|3d_{ij}\uparrow\rangle\neq 0$ whereas $\langle 2p_\pi\downarrow|3d_{ij}\uparrow\rangle=0$, the σ bonding of the oxygen with the $|sp^3\rangle$ hybrid states of the La^{3+} ion[9] will be preferentially produced by the electron that tries to keep apart from the $|3d_{ij}\rangle$ Mn orbitals. A Fermi contact spin polarization[14] is thus produced at the position of the La nucleus with a hyperfine field $B_N\approx 35$ kG as shown below. The dipolar term in Eq. (1) has a smaller contribution to the local field of the order of a few kG, which however is crucial in the determination of the experimental results.

Returning to Fig. 2, it is observed that below T_c, a single broad line appears, which becomes stronger by decreasing temperature down to $T=180$ K where it starts to decrease. At $T\approx 200$ K a second higher-frequency signal appears which on cooling appears to increase slightly. It is further observed that at low temperatures the frequency peaks of the two lines get closer to each other. This behavior becomes more apparent in Figs. 3(a) and 3(b) which demonstrate the local field $B_l=|\mathbf{B}_N+\mathbf{B}_d|=\omega_L/\gamma$ and the signal intensity I versus T for both lines, as obtained by the spectral areas of a

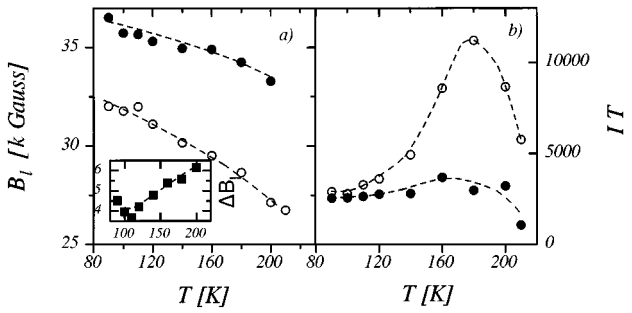

FIG. 3. (a) The local magnetic field at the La site $B_l = \omega_L / \gamma$ as a function of temperature. The lower curve (open circles) corresponds to ferromagnetically ordered Mn octants, whereas the higher curve (filled circles) corresponds to antifferomagnetically ordered Mn octants. The inset presents the difference $\Delta B_l = B_l(\mathrm{AFM}) - B_l(\mathrm{FM})$. (b) The ^{139}La NMR signal intensity I, corrected by the Boltzmann factor, as a function of temperature. The signal intensities are obtained from the spectral areas of two-Gaussian line-shape fits. The filled circles correspond to the AFM signal, whereas the open circle corresponds to the FM signal.

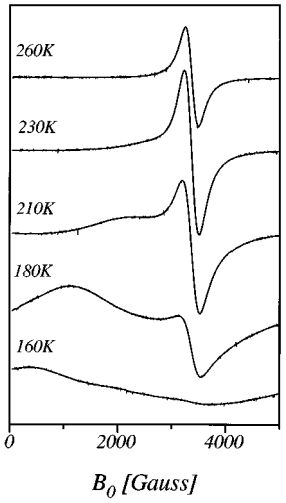

FIG. 4. Mn^{4+} X-band EPR spectra at various temperatures above and below $T_c \approx 235$ K.

two-Gaussian line-shape fit. The signal intensities have been corrected by the Boltzmann factor in order to get the correct temperature dependence of I.

A comparison of Figs. 1 and 3(b) shows a remarkable similarity between the M versus T curve and the I versus T curve which corresponds to the low B_l field component, in the FM phase. This suggests that the La nuclei with the lower $B_{/\!/}$ field are located at the center of ferromagnetically ordered Mn spin octants, contrary to the expectation that FM ordering should create the strongest B_l field at the position of the La sites. Besides, the difference between the two local fields lies in the range $\Delta B_l \approx 4-6$ kG, which is of the order of the dipolar contribution to the local field.[12] These facts are nicely explained if we assume that the La ions which sense the higher $B_{/\!/}$ field are placed at the center of antiferromagnetically ordered spin octants while at the same time, (i) $B_N(\mathrm{AFM}) \approx B_N(\mathrm{FM})$, and (ii) in the FM octants $B_d(\mathrm{FM})$ is antiparallel to $B_N(\mathrm{FM})$, thus leading to relatively lower $B_{/\!/}(\mathrm{FM})$ values than in the AFM octants where $B_d(\mathrm{AFM}) \approx 0$. The slightly different temperature variation of $B_{/\!/}(\mathrm{FM})$ with respect to $B_{/\!/}(\mathrm{AFM})$—shown in the inset of Fig. 3—can be interpreted as a small decrease of the dipolar contribution due to the partial transformation of the spin alignment from FM to AFM ordering. This description is consistent with synchrotron XRD data in $La_{0.5}Ca_{0.5}MnO_3$ (Ref. 7) and neutron diffraction data in $Pr_{0.5}Sr_{0.5}MnO_3$.[15] Furthermore, the two different spin alignments for $T < T_N$ are in agreement with the double spin-cell CE structure.[8,9] However, the spin cell which is responsible for $B_{/\!/}(\mathrm{FM})$—probably the E type spin cell[18]—has a nonvanishing B_d contribution at the La sites, i.e., it is partially ferromagnetically ordered (PFO).

It is worth it to notice that due to the cubic symmetry one should expect a vanishing small $B_N(\mathrm{AFM})$. The observed strong AFM signals point out that the hyperfine field is not symmetrically transferred from the Mn octant. This might result from the $|sp^3\rangle$ hybrid La orbitals[9] which stablilize the O-La bonding by breaking the cubic symmetry, or the Jahn-Teller distortion of the oxygen octahedra.

An interesting feature in Fig. 3(a) is that both $B_{/\!/}(T)$ curves do not tend to zero for $T \to T_c$ but retain high $B_{/\!/}(T_c)$ values, about 80% of the corresponding maximum values. A similar result has been reported in Ref. 12 in closely related compounds. This effect, in conjunction with the rapid decrease of the FM signal intensity for $T \to T_c$, indicates that in the temperature region $180 \leqslant T \leqslant T_c$ a paramagneticlike component appears, where a frozen spin alignment is no more energetically favored. The presence of a PM component is directly confirmed by X-band Mn^{4+} EPR measurements (Fig. 4), according to which the high-temperature PM signal penetrates deeply into the FM phase. For $T > T_c$ the EPR PM signal rapidly increases down to T_c, where it starts decreasing until it disappears at $T \approx 160$ K. The appearance of a second broad signal for $T < 220$ K can be attributed to the FM phase. It looks as if ordered groups of spins start to fluctuate coherently, while at T_c the spin-fluctuating regions cover the whole FM phase. The presence of a PM component for $T < T_c$ has been also observed in $La_{0.67}Ca_{0.33}MnO_3$ with neutron scattering techniques,[16] and in $La_{0.75}Ca_{0.25}Mn_{0.98}Fe_{0.02}O_3$, as well as in $La_{0.67}Ca_{0.33}Mn_{0.99}Fe_{0.01}O_3$ by using Mössbauer spectroscopy.[17] Furthermore, both techniques have shown that by increasing temperature towards T_c, the fraction of the PM phase increases in a similar fashion with the EPR results.

The assumption for the existence of a PFO spin cell for $T < T_N$ is further supported by NMR signal amplitude A_S versus the rf field B_1 measurements performed at different spectral frequencies and at various temperatures, in both the FM and the AFM phases [Figs. 5(a) and 5(b)]. The intense NMR signals observed at very low rf power levels are due to the strong enhancement factor n which originates from the oscillations of the local electronic moments at the rf frequency. In this way, the actual rf field is not the weak applied field B_1 but a stronger one produced by the oscillating electron magnetic moments. At $T = 180$ K, A_S for both the strong FM and the small AFM signals follows the same asymmetric bell-shaped curve given by the relation[11]

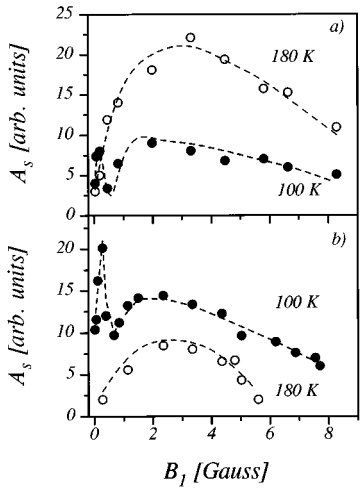

FIG. 5. The signal amplitude A_S vs the rf field B_1 at two different spectral frequencies, (a) at 18 MHz corresponding to the FM line, for $T=180$ K$>T_N$ (open circles) and $T=100$ K$<T_N$ (filled circles); (b) at 21 MHz corresponding to the AFM line, for $T=180$ K$>T_N$ (open circles) and $T=100$ K$<T_N$ (filled circles). Dashed lines are guide to the eye.

$$A_S \propto n \sin(n\gamma B_1 \tau)\sin^2\left(\frac{n\gamma B_1 \tau}{2}\right), \tag{2}$$

which attains a maximum at $n\gamma B_1\tau = 2\pi/3$.[19] Using this formula and the fact that the maximum appears at $B_1 \approx 3$ G a large enhancement factor $n \sim 3\times 10^2$ is obtained. Usually, such high- n values characterize NMR signals arising from magnetic domain walls.[10] For $T<T_N$ the maximum is slightly shifted at $B_1 \approx 2$ G, while a second maximum appears corresponding to an even stronger enhancement factor $n \approx 2\times 10^3$. In order to discriminate the origin of the two different n contributions, a two-Gaussian line-shape analysis has been performed at $T=90$ K for rf fields $B_1 \approx 0.5$ and 2 G (Fig. 6). For $B_1 \approx 0.5$ G the AFM signal contribution is considerably higher than for $B_1 \approx 2$ G. It is thus clear that the strong n component can be attributed to the higher-frequency AFM signal, whereas the lower n component can

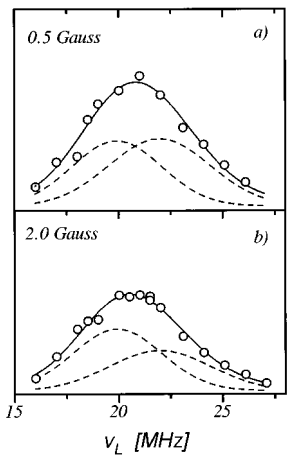

FIG. 6. ^{139}La NMR spectra at $T=90$ K, for $B_1=0.5$ and 2 G. In each case the solid lines are fits resulting from the sum of the two-Gaussian dashed lines.

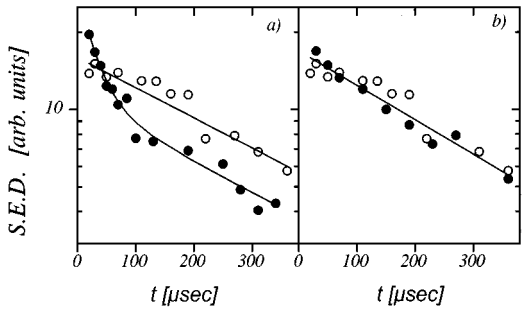

FIG. 7. (a) Spin-echo decays at $T=90$ K and frequency 21 MHz (AFM line). The double exponentially decaying curve (filled circles) corresponds to $B_1=0.5$ G whereas the single exponential curve (open circles) corresponds to $B_1=2$ G. (b) Comparison of spin-echo decays for (i) $B_1=2$ G, $T=90$ K, frequency 21 MHz (open circles) and (ii) $B_1=3$ G, $T=180$ K, frequency 18 MHz (filled circles).

be attributed to the low-frequency FM signal. Furthermore, for $B_1 \approx 0.5$ G the obtained signal-intensity ratio $I(\mathrm{FM})/I(\mathrm{AFM}) \approx 1$ as expected for a double-cell spin configuration.

A third evidence about the presence of PFO for $T<T_N$ is obtained by using spin-spin relaxation-time T_2 measurements. Figure 7(a) shows the spin-echo decays (SED) at spectral frequency 21 MHz, $T=90$ K, and rf levels $B_1=0.5$ and 2 G. It is observed that the low-rf SED is decaying with a double exponential with relaxation times, $T_{2,A}=80$ μsec, and $T_{2,B}=650$ μsec, whereas the high-rf SED is single exponential with $T_2 \approx T_{2,B}$. Figure 7(b) compares the SED at 90 K, spectral frequency 21 MHz, and $B_1=2$ G with the FM SED at 180 K, spectral frequency 18 MHz, and $B_1=3$ G. It is found that $T_2(180\ \mathrm{K}) \approx T_{2,B} \approx 650$ μsec. These results, in conjunction with the analysis of Fig. 6 indicate that antiferromagnetically coupled spins relax with the short $T_{2,A}$, while ferromagnetically coupled spins relax with the long $T_{2,B}$.

Considering that the spin-spin relaxation originates from indirect Suhl-Nakamura interactions[20] between couples of nuclear spins we get $T_2 \propto (J/A^2)$, where J is an effective Mn-Mn exchange-coupling constant. Since A mainly depends on atomic properties and the lattice cell geometry, the similar T_2 values of the low-frequency FM NMR lines in both the FM and AFM phases indicate similar exchange-coupling constants, i.e., that the low-field spin cell is PFO, even for $T<T_N$. If we consider that DE overrules coupling into the FM regions while superexchange (SE) into the AFM ones, the lower T_{2A} values indicate that DE coupling is, as expected, sufficiently stronger than the AFM superexchange coupling.

IV. DISCUSSION

We anticipate that the above experimental results are evidence that the low-temperature double-cell spin configuration consists of PFO and AFM cells, where DE and SE dominate, respectively. The gradual shift of $B_{/\!/}$(FM) to $B_{/\!/}$(PFO), when related to the electron microscopy results,[4] indicates not only the subsequent transformation of the ferromagnetically ordered Mn spin octants to PFO, but also that

the DE interactions become more localized.

The possibility of a structure with alternating stacked FM and AFM spin cells has been theoretically predicted many years ago.[21] In the nearest-neighbor approximation, the Hamiltonian which describes these La based perovskites and related structures, includes t_{2g}-e_g spin-exchange, vacancy hopping, and t_{2g}-t_{2g} spin-exchange terms,

$$H=-J_H\sum\ (\mathbf{S}\boldsymbol{\sigma})_{\alpha\beta}c^*_{i\beta}c_{i\beta}+t\sum\ c^*_{i\alpha}c_{j\alpha}-J\sum\ S_iS_j\,, \tag{3}$$

where $c^*_{i\alpha}, c_{i\alpha}$, are creation and annihilation operators for the ''conduction'' e_g electrons, i,a are their coordinate and spin projection, and S_i is the spin operator of the t_{2g} electrons. The second term in Eq. (3) transfers the e_g electron to the next Mn^{4+} site while conserving its spin projection, so if the spins S_i, and $S_{i\pm1}$ are antiparallel, the electron transfer should increase the energy by an amount $|J_H|S$. In the case of parallel S_i and $S_{i\pm1}$ spins, the energy will be decreased by the same amount, thus establishing DE.

Considering a continuum approximation of Hamiltonian (3), where spatial-charge fluctuations are taken into consideration, Kashin and Nagaev[21] have shown that for a conduction bandwidth $W=2zt\gg|J_H|S$ and carrier concentration $x\geqslant x_F=4|J|/|J_H|$ per unit cell volume, the ground state of Hamiltonian (3) consists of alternating regions with increased (FM) and decreased (AFM) electron densities. It is interesting to notice that if we consider that $|J|/|J_H|=T_{2,A}/T_{2,B}\approx1/8$, we get $x_F\approx0.5$ in agreement with the experiments which show that charge ordering appears only for $x\geqslant0.5$. This might be a coincidence because the model is oversimplified with respect to the real system, but we think it deserves a more careful examination. The incommensurate CO superstructure, observed with electron microscopy, could be thus explained as stemming from an ordered FM-AFM domain lattice, which at low temperature transforms to the observed two-cell stacked spin structure. This behavior closely resembles the insulating AFM phase of the copper-oxide-based high-T_c superconductors. Schulz applied the Hartree-Fock theory on a two-dimensional Hubbard model[22] in the vicinity of half filling of the conduction band and proved that the commensurate AFM state is unstable against domain-wall formation thus leading to the establishment of an incommensurate insulating state, with the extra carriers localized on the domain walls.

In conclusion, ^{139}La NMR measurements in conformity with magnetic and EPR measurements indicate (i) the low-temperature AFM phase of $La_{0.5}Ca_{0.5}MnO_3$ consists of stacked AFM and PFO spin octants which are formed by the subsequent transformation of a mixed FM/AFM phase, and (ii) the PM-FM phase transition is driven by unusual coherent spin fluctuations which are present at least down to $T\approx180$ K.

ACKNOWLEDGMENTS

Fruitful discussions with Dr. C. Papatriantafilou and Dr. C. Christides are greatly acknowledged.

[1] P. Schiffer, A. P. Ramirez, W. Bao, and S.-W. Cheong, Phys. Rev. Lett. **75**, 3336 (1995).
[2] Y. Tomioka, A. Asamitsu, Y. Moritomo, H. Kuwahara, and Y. Tokura, Phys. Rev. Lett. **74**, 5108 (1995).
[3] A. P. Ramirez, P. Schiffer, S.-W. Cheong, C. H. Chen, W. Bao, T. T. M. Palstra, P. L. Gammel, D. J. Bishop, and B. Zegarski, Phys. Rev. Lett. **76**, 3188 (1996).
[4] C. H. Chen and S.-W. Cheong, Phys. Rev. Lett. **76**, 4042 (1996).
[5] C. Zener, Phys. Rev. **82**, 403 (1951); P. G. de Gennes, *ibid.* **118**, 141 (1960).
[6] A. J. Millis, P. B. Littlewood, and B. I. Shraiman, Phys. Rev. Lett. **74**, 5144 (1995).
[7] P. G. Radaelli, D. E. Cox, M. Marezio, S.-W. Cheong, P. E. Schiffer, and A. P. Ramirez, Phys. Rev. Lett. **75**, 4488 (1995).
[8] E. O. Wollan, and W. C. Koehler, Phys. Rev. **100**, 545 (1955).
[9] J. B. Goodenough, Phys. Rev. **100**, 564 (1955).
[10] M. B. Stearns, Phys. Rev. **162**, 496 (1967); A. C. Gossard and A. M. Portis, Phys. Rev. Lett. **3**, 164 (1959).
[11] H. G. Bohn, R. R. Arons, and H. Lütgemeier, Physica **80B**, 6 (1975).
[12] M. K. Gubkin, T. A. Khimich, E. V. Kleparskaya, T. M. Perekalina, A. V. Zalessky, J. Magn. Magn. Mater. **154**, 351 (1996); M. K. Gubkin, A. V. Zalessky, V. G. Krivenko, T. M. Perekalina, T. Khimich, and V. A. Chubarenko, Pis'ma Zh. Eksp. Teor. Fiz. **60**, 56 (1994) [JETP Lett. **60**, 57 (1994)].
[13] R. G. Shulman, and K. Knox, Phys. Rev. **119**, 94 (1960).
[14] The creation of a contact term in nonmagnetic nuclei is nicely described in A. J. Freeman, and R. E. Watson, Phys. Rev. Lett. **6**, 343 (1961); R. G. Shulman and K. Knox, *ibid.* **4**, 603 (1960).
[15] K. Knizek, Z. Jirak, E. Pollert, F. Zounova, and S. Vratislav, J. Solid State Chem. **100**, 292 (1992).
[16] J. W. Lynn, R. W. Erwin, J. A. Borches, Q. Huang, A. Santoro, J.-L. Peng, and Z. Y. Li, Phys. Rev. Lett. **76**, 4046 (1996).
[17] M. Pissas, G. Kallias, E. Devlin, A. Simopoulos, and D. Niarchos, J. Appl. Phys. (to be published); A. Simopoulos, G. Kalias, A. Devlin, M. Pissas, and D. Niarchos (unpublished).
[18] According to Refs. 8 and 9, the *E*-type spin octants form only for $x\approx0.5$. For higher Ca concentrations the *E* octants subsequently transform to *C* octants, while for $x>0.75$ the system is antiferromagnetically ordered with a *C*-type spin-lattice.
[19] Complications in the applications of Eq. (2) arise from the fact that generally n depends on B_1. However, an average $\langle n\rangle$ can be obtained from the intensity maximum which occurs at $n\gamma B_1\tau=2\pi/3$.
[20] H. Suhl, Phys. Rev. **109**, 606 (1958); T. Nakamura, Prog. Theor. Phys. **20**, 547 (1958); D. Hone, V. Jaccarino, and T. Ngwe, Phys. Rev. **186**, 291 (1969).
[21] V. A. Kashin, and E. L. Nagaev, Zh. Eksp. Teor. Fiz. **66**, 2105 (1974) [Sov. Phys. JETP **39**, 1036 (1974)]; E. L. Nagaev, Pis'ma Zh. Eksp. Teor. Fiz **16**, 558 (1972) [JETP Lett. **16**, 394 (1972)].
[22] H. J. Schulz, Phys. Rev. Lett. **64**, 1445 (1990).